Geophysical Journal International

Geophys. J. Int. (2015) **203,** 1896–1908 doi: 10.1093/gji/ggv419
GJI Seismology

Comparison of the STA/LTA and power spectral density methods for microseismic event detection

Yoones Vaezi and Mirko Van der Baan

Department of Physics, University of Alberta, Edmonton, AB T6G 2E1, Canada. E-mail: yvaezi@ualberta.ca

Accepted 2015 September 28. Received 2015 August 7; in original form 2015 March 21

SUMMARY

Robust event detection and picking is a prerequisite for reliable (micro-) seismic interpretations. Detection of weak events is a common challenge among various available event detection algorithms. In this paper we compare the performance of two event detection methods, the short-term average/long-term average (STA/LTA) method, which is the most commonly used technique in industry, and a newly introduced method that is based on the power spectral density (PSD) measurements. We have applied both techniques to a 1-hr long segment of the vertical component of some raw continuous data recorded at a borehole geophone in a hydraulic fracturing experiment. The PSD technique outperforms the STA/LTA technique by detecting a higher number of weak events while keeping the number of false alarms at a reasonable level. The time–frequency representations obtained through the PSD method can also help define a more suitable bandpass filter which is usually required for the STA/LTA method. The method offers thus much promise for automated event detection in industrial, local, regional and global seismological data sets.

Key words: Time-series analysis; Fourier analysis.

1 INTRODUCTION

Microseismic monitoring is a term commonly used to refer to methods that include the acquisition of continuous seismic data for locating and characterizing microseismicity induced by oilfield completion and production processes. This information can further be used for monitoring resulting reservoir changes and understanding the associated geomechanical processes in the subsurface. It is not only considered as the only technology for hydrofracture monitoring, but is also known to have proven useful for geothermal studies, reservoir surveillance, and monitoring of CO_2 sequestration (Phillips *et al.* 2002; Maxwell *et al.* 2004; Warpinski 2009; van der Baan *et al.* 2013). Here the term 'microseismicity' is defined as seismicity of magnitude less than 0 (Maxwell *et al.* 2010) and should be distinguished from the terms 'microtremor' or 'microseism' that commonly refer to more or less continuous motion with a period of 4 to 20 s in the Earth that is unrelated to an earthquake (Ewing *et al.* 1957; Lee 1935).

One of the main processing steps that is of paramount importance for accurately monitoring spatio-temporal distribution of microfractures is in fact to first detect these events. Since microseismic data are mostly acquired continuously they usually comprise large volumes. Likewise, earthquake monitoring can lead to large data volumes simply because many instruments can be operational over a long time span. Such large volumes of data call for an automatic event detection algorithm to replace manual detection, which is highly subjective and time consuming. Numerous automatic trigger algorithms are available which are generally characterized into time domain, frequency domain, particle motion processing, or pattern matching (Withers *et al.* 1998). They are all either based on the envelope, the absolute amplitude, or the power of signals in the frequency or time domains.

Although there are many sophisticated trigger methods they usually require complicated parameter adjustments to reflect actual signal and noise conditions at each seismic site. Finding suitable parameters has proven unwieldy and subject to error. Therefore, in practice, only relatively simple trigger algorithms have been really broadly accepted and can be found in seismic data recorders in the market and in most real-time processing packages. Among all, the short-term average/long-term average (STA/LTA) technique (Allen 1978) continues to remain as the most popular method in which the ratio of continuously calculated average energy (or envelope or absolute amplitude) of a recorded trace in two consecutive moving-time windows, a short-term window and a subsequent long-term window (STA/LTA ratio), is used as a criterion for picking. However, this method has also its own disadvantages. For instance, it requires careful setting of parameters (Trnkoczy 2002) including a trigger threshold level and two window lengths (both short- and long-term windows). A low threshold can lead to many false triggers (false positives) while a high threshold may result in missing weak events (false negatives).

High sensitivity to the signal-to-noise ratio (S/N) level is a common shortcoming among various event detection algorithms. This may cause the weak events whose energies and amplitudes are

comparable to the background noise to be obscured in the presence of strong noise and go untriggered. In this paper, we have compared the performance of two event detection methods, a modified version of the power spectral density (PSD) technique introduced by Vaezi & van der Baan (2014) and the STA/LTA algorithm, when applied to 1-hr long single-trace data recorded by the vertical channel of a geophone in a borehole array in a microseismic experiment. We conclude that compared to the STA/LTA method, the PSD technique not only detects a larger number of weak events at a still tolerable number of false triggers, but also helps design a more suitable bandpass filter for further analysis of microseismic data, whereas the STA/LTA method usually requires the data to be bandpassed prior to event detection. We also suggest that the PSD method would perform relatively better in triggering emerging events where the gradual amplitude increase can cause the STA/LTA method to fail.

2 METHODOLOGY

The idea behind the STA/LTA method is simple; the STA/LTA ratio is calculated continuously at each time t for every kth data channel x_t as $R = \frac{\text{STA}}{\text{LTA}}$, where

$$\text{STA} = \frac{1}{N_S}\sum_{n=1}^{N_S} y_{k,n}, \tag{1}$$

and

$$\text{LTA} = \frac{1}{N_L}\sum_{n=-N_L}^{0} y_{k,n}. \tag{2}$$

The STA is the N_S-point short-term average and the LTA is the N_L-point long-term average. Note that we have considered non-overlapping STA and LTA windows. The parameter y_t is the characteristic function (CF) $y_t = g(x_t)$, which is devised in such a way that it enhances the signal changes. The common CF choices include energy ($y_t = x_t^2$) (McEvilly & Majer 1982), absolute value ($y_t = |x_t|$) (Swindell & Snell 1977) and envelope function ($y_t = \sqrt{x_t{}^2 + h(x_t)^2}$, where h denotes Hilbert transform) (Earle & Shearer 1994). The STA measures the instantaneous amplitude level (or other CF) of the seismic signal and watches for events while the LTA takes care of the current average seismic noise amplitude (or other CF). When the ratio (R) of y_t exceeds a predetermined (user-selected) threshold τ, a detection is declared. The trigger is active until the ratio falls below a detrigger threshold (Trnkoczy 2002). Although they can be different, the trigger and detrigger thresholds are commonly taken to be equal and are simply called the detection threshold ($\tau > 1$). The most important STA/LTA trigger algorithm parameters are thus the STA and LTA window lengths (N_S and N_L), and the detection threshold (τ).

For an event to be detected by the STA/LTA method, its energy (amplitude) should be adequately higher than that of the background noise. This simply may not be always true for weak events. Also the STA/LTA method is commonly applied to data which are bandpassed over a frequency range where signal dominates with respect to the background noise. But in general, for energy detectors (such as STA/LTA method) no single filter will be optimal for a large variety of signals in a dynamic noise environment.

An alternative to this problem is to analyse the time-series in the frequency domain. In order to detect events in a relatively stationary noise condition, Vaezi & van der Baan (2014) use the fact that the microseismic events typically represent stronger spectral content over a frequency band (narrow or wide, depending on the nature of the event) than that of the background noise. The main steps involved in this technique are described here.

Assume a continuous data record $x(t)$ that is stationary with average $\overline{x} = 0$. First the average PSD of the seismic background noise, $\overline{PSD}(f)$, is estimated using a Welch method (Welch 1967; McNamara & Buland 2004), which is known to reduce the variability of spectral estimates. By removing the energetic events, transients and any types of noise bursts we consider only the noise at quiet times, $x'(t)$, to calculate the average noise PSD (Peterson 1993). A quiet version of the data record can be roughly obtained by discarding samples of absolute amplitudes greater than a multiple of the original record's root-mean-square (RMS) amplitude (Fig. 1). The quiet noise record is divided into M overlapping segments, $x'_m(t_l)$, each of length L, with $m = 1, 2, ..., M$ and $l = 1, 2, ..., L$, using windowing tapers of length L. The total average PSD is then calculated by averaging the one-sided PSD estimates over all the individual background noise segments:

$$\overline{PSD}(f) = \frac{1}{M}\sum_{i=1}^{M} \text{PSD}'_m(f), \tag{3}$$

where $\text{PSD}'_m(f)$ stands for the PSD estimate of the mth noise segment as a function of frequency f given by:

$$\text{PSD}'_m(f) = \begin{cases} \dfrac{a\left|\sum_{l=1}^{L} x'_m(t_l)w(t_l)e^{-j2\pi fl}\right|^2}{f_s L U} & \text{if} \quad f = 0, f_{\text{Nyq}} \\ \dfrac{2a\left|\sum_{l=1}^{L} x'_m(t_l)w(t_l)e^{-j2\pi fl}\right|^2}{f_s L U} & \text{if} \quad 0 < f < f_{\text{Nyq}} \end{cases} \quad m = 1, 2, ..., M, \tag{4}$$

where a is a scale factor that accounts for variance reduction which depends on the type of the taper w, f_{Nyq} is the Nyquist frequency in Hz, f_s is the sampling frequency in Hz, $j = \sqrt{-1}$ and U is the window normalization constant that ensures the modified periodograms are asymptotically unbiased and is given by

$$U = \frac{1}{L}\sum_{i=1}^{L} w(t_i)^2. \tag{5}$$

The standard deviations are also calculated at each frequency of the average PSD. As there are no redundant components in the Fourier transforms at the frequencies of 0 and f_{Nyq}, the PSD estimates at these frequencies do not double in eq. (4) when converting the two-sided PSD estimates to one-sided PSDs, as opposed to those in the frequency range of $0 < f < f_{\text{Nyq}}$.

In the next step, the original data $x(t)$ are similarly divided into N overlapping segments of length L. In other words, a rolling window of predetermined length L is used to compute the PSD for each windowed segment throughout the original data $x(t)$:

$$\text{PSD}_n{}^t(f) = \begin{cases} \dfrac{a\left|\sum_{l=1}^{L} x_n(t_l)w(t_l)\text{e}^{-j2\pi fl}\right|^2}{f_s L U} & \text{if} \quad f = 0, f_{\text{Nyq}} \\ \dfrac{2a\left|\sum_{l=1}^{L} x_n(t_l)w(t_l)\text{e}^{-j2\pi fl}\right|^2}{f_s L U} & \text{if} \quad 0 < f < f_{\text{Nyq}} \end{cases} \quad n = 1, 2, ..., N. \tag{6}$$

The purpose of using tapers is to suppress side-lobe spectral leakage and also reduce the bias of the spectral estimates. However, they increase the width of the main lobe of the spectral window, therefore reducing the resolution. There is always a trade-off between variance reduction and resolution as long as single data tapers are used for spectral estimations (Park *et al.* 1987). There are several types of tapers available with different variance and resolution properties

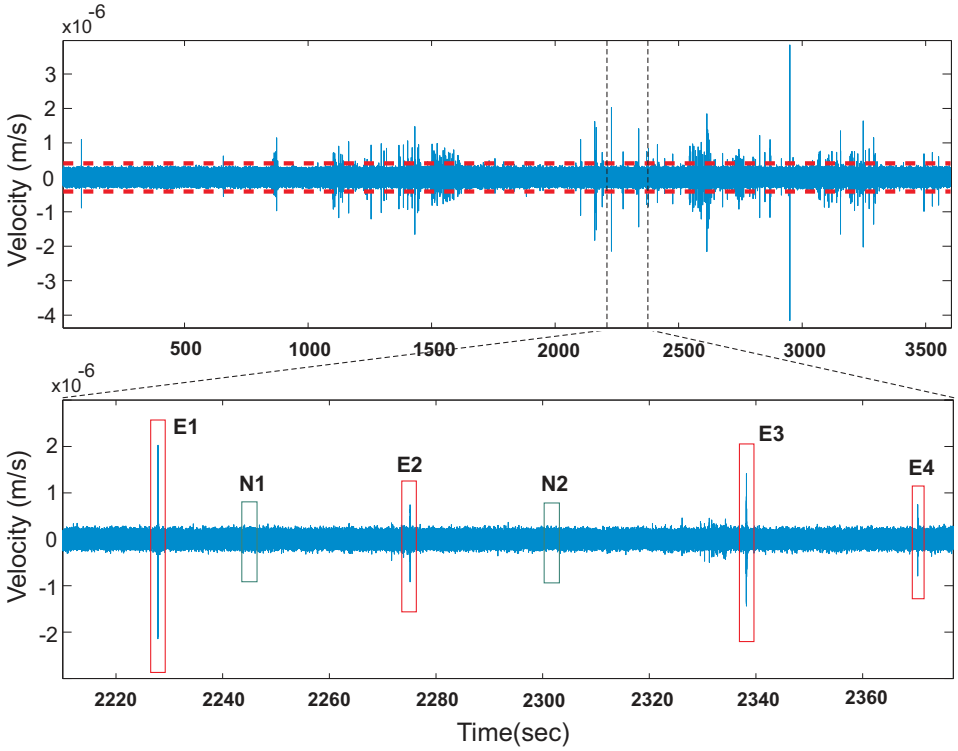

Figure 1. The *Z*-component of a 1-hr long segment of the raw continuous microseismic data and its zoomed view in which four events E and two background noise segments N are denoted by red and green boxes, respectively. The PSD estimates of these features are compared with the average PSD in Fig. 2. Only the data in the region between the two red dashed lines (here with an absolute amplitude of five times the root-mean-square amplitude) are used when calculating the average noise PSD.

(Harris 1978). The Hanning and cosine tapers are the two most commonly used tapers. In this paper we use Hanning taper which has a relatively high variance but with very good spectral leakage properties (Park *et al.* 1987). Although applying moving average filters to single-taper spectral estimates reduces the variance, it adversely increases the bias of the estimate due to short-range loss of frequency resolution (Park *et al.* 1987). However, instead of single-taper estimations which suffer from relatively high variance, one can use the multitaper spectral estimation method to provide a more consistent estimate with lower variance. In this technique, a single spectral estimate is formed by combining several eigenspectra obtained by taking discrete Fourier transform of the product of several leakage-resistant tapers with the data (Thomson 1982; Park *et al.* 1987). However, even multitaper analysis cannot fix the variability caused by non-stationary noise components of high amplitudes that, if present, may obscure the variability due to single data tapers.

The average PSD is then subtracted from all individual PSDs:

$$\text{misfit}_n{}^t(f) = \text{PSD}_n{}^t(f) - \overline{PSD}(f), \tag{7}$$

where $\text{misfit}_n{}^t(f)$ stands for the PSD difference at each time t associated with the middle point of the nth segment as a function of frequency f, which is hereafter denoted by $\text{misfit}_t(f)$ for simplicity, $\text{PSD}_n{}^t(f)$ denotes the individual PSD at the corresponding time and $\overline{PSD}(f)$ is the calculated average PSD. These differences are then divided by standard deviations at each frequency to calculate the normalized PSDs $u_t(f)$ as:

$$u_t(f) = \frac{\text{misfit}_t(f)}{\text{std}(f)}, \tag{8}$$

where $\text{std}(f)$ is the standard deviation at frequency f computed from the PSDs of each noise segment $\text{PSD}'_m(f)$ analogous to eq. (3). The resulting time–frequency representation highlights then all signals that stand out in a statistical sense from the reference spectrum, in this case the background noise. The ratios that are below 1 are set to zero to have a clearer depiction of the events:

$$\Gamma_t(f) = \begin{cases} u_t(f) & \text{if} \quad u_t(f) > 1 \\ 0 & \text{otherwise} \end{cases}. \tag{9}$$

In other words, Vaezi & van der Baan (2014) suggest that any short time segment with a PSD statistically larger than the average PSD by some likelihood threshold includes a potential event. Both transient and persistent events are detectable by this method. This method can also be used for detecting individual frequency bands that are statistically above the average threshold, and subsequently determining suitable bandpass filters. In the next step, an averaged PSD criterion is calculated by summing the computed quantities $\Gamma_t(f)$ over all frequencies and dividing them by the number of frequencies:

$$\Lambda_{\text{PSD}}(t) = \frac{\sum_{f=0}^{f_{\text{Nyq}}} \Gamma_t(f)}{N_f}, \tag{10}$$

where $\Lambda_{\text{PSD}}(t)$ is the averaged version of the PSD detection criterion as a function of time, f_{Nyq} represents the Nyquist frequency and N_f is the total number of frequencies. Another alternative approach is to use the average of $\Gamma_t(f)^2$s as the triggering criterion:

$$\Phi_{\text{PSD}}(t) = \frac{\sum_{f=0}^{f_{\text{Nyq}}} \Gamma_t(f)^2}{N_f}. \tag{11}$$

When the $\Lambda_{\text{PSD}}(t)$ (or $\Phi_{\text{PSD}}(t)$) becomes larger than a predetermined value, say λ_{PSD} (or ϕ_{PSD}), an event is declared. Assuming a Gaussian distribution, for any selected λ_{PSD}, the probability in

Table 1. The parameters used for the STA/LTA and PSD detection methods.

STA/LTA parameters		PSD parameters	
STA window length	30 ms (120 samples)	PSD window length	0.25 s (1000 samples)
LTA window length	100 ms (400 samples)	Window overlap	50 per cent
Minimum event separation	0.5 s	Minimum event separation	0.5 s
Minimum event duration	50 ms		
STA/LTA detection threshold	2.00	PSD detection threshold	0.065

percentages that a trigger with a measured averaged PSD criterion of $\Lambda_{\mathrm{PSD}}(t)$ at time t is due to noise can be calculated by:

$$Pr\{\Lambda_{\mathrm{PSD}} \text{ is noise} | \Lambda_{\mathrm{PSD}} = \Lambda_{\mathrm{PSD}}(t)\} = \frac{1}{2}\left(1 - \mathrm{erf}\left(\frac{\Lambda_{\mathrm{PSD}}(t) - \mu}{\sigma\sqrt{2}}\right)\right) \times 100 \text{ per cent}, \quad (12)$$

where μ and σ are the mean and standard deviation for the $\Lambda_{\mathrm{PSD}}(t)$ and erf(x) is the error function (Andrews 1997) defined as:

$$\mathrm{erf}(x) = \frac{2}{\sqrt{\pi}} \int_0^x \mathrm{e}^{-t^2}\, \mathrm{d}t. \quad (13)$$

3 DATA SET

The data set we have used for this study consists of a 1-hr segment out of 44-hr long continuous borehole microseismic data which were acquired to monitor multistage fracture treatments taking place at two horizontal wells for the purpose of increasing the formation permeability of a tight gas reservoir. The borehole array consists of 12 triaxial conventional 15-Hz geophones deployed in a vertical monitoring borehole, which is located between the two injection wells (Eaton *et al.* 2014). The sampling time interval is 0.25 ms. For simplicity we have considered the vertical component of the shallowest receiver (receiver 1) only. Fig. 1 shows the data segment used for the current analysis.

4 RESULTS

The parameters shown in Table 1 are used to calculate the STA/LTA ratios and the PSD criterion (Vaezi & van der Baan 2014). The detection thresholds in both methods are selected in such a way that they give the best balance between the false alarms and missed events. The minimum event separation specifies the minimal time length between the end of the previous active triggering and the beginning of the current triggering. When two detections are very close in time, this parameter decides if they should be considered as two separated phases or not. The minimum event duration for the STA/LTA method is the minimal time length between the time of an event triggering and the time of detriggering. In other word, this parameter specifies the minimum duration of a seismic phase to be detected. If this parameter is very small, it becomes increasingly possible to misidentify an instrument glitch (a spike) as a seismic phase.

The average PSD is calculated using the same PSD window length and overlap as in Table 1 via a modified Welch method (McNamara & Buland 2004). In order to prevent the energetic events, transients and any types of noise bursts to bias the average noise PSD estimation, we simply removed the samples with absolute amplitudes greater than five times the RMS amplitude of the entire raw trace (red dashed lines in Fig. 1). Therefore, we roughly consider only the noise at quiet times to calculate the average noise PSD. Fig. 2 shows the average PSD curve ($\overline{PSD}(f)$ in eq. 3) in black along with the calculated standard deviations at each frequency (std(f) in eq. 8) in red bars. To better show how the PSD method works, this figure shows also the PSD estimates for four different microseismic events (red boxes in Fig. 1) and two noise segments randomly selected from some quiet region of the data (green boxes in Fig. 1) in different colours. Note that all event PSDs exceed the average PSD, especially at the frequencies below 120 Hz, while the sample noise PSDs lie mostly within one standard deviation. This property is used to detect microseismic events using the PSD technique. The spectral peaks observed at the frequency of 60 Hz and its multiples are related to the 60-Hz electric noise and its harmonic overtones. A frequency tolerance equal to two times the Rayleigh resolution (Harris 1978) for the Hanning tapers used in this analysis is considered to discard the PSD ratios calculated around these frequencies and also to account for slight variability in the frequencies at which the harmonics are expected to appear.

Fig. 3(a) shows the time–frequency representation of the calculated $u_t(f)$ (eq. 8). Fig. 3(b) shows the thresholding function $\Gamma_t(f)$ (eq. 9) where the microseismic events are more evident, particularly in the frequency band of [0 120] Hz. Figs 4(a) and (b) show the calculated STA/LTA ratios and PSD criterion using the parameters listed in Table 1, respectively. The detection thresholds are plotted as red dashed lines in each figure.

The PSD method is applied to the raw data in Fig. 1 and the STA/LTA technique is applied to the same data filtered with two narrow notch filters implemented at the frequencies of 60 and 120 Hz. The total number of triggered events by the PSD technique is 897, which is more than two times the total number of events triggered by the STA/LTA method that is 412 events. All the events triggered by both techniques are manually inspected in order to separate the false alarms (false positives) from the true positives (real events) and to statistically compare the performance of the two detection algorithms. In addition to microseismic events, any other coherent features recorded along the borehole array that may be of interest to an interpreter, such as low-frequency signals within regional events (small earthquakes) or long-period long-duration (LPLD) events (Das & Zoback 2013; Caffagni *et al.* 2015), are also considered as true positives. Here, we refer to all these types of real events as 'master events'.

The first two rows in Table 2 compare the number of master events (microseismic or regional events), false alarms and missed events in the two detection methods when applied to the corresponding data. Here, since all the master events detected by the STA/LTA method are also detected via the PSD technique, the latter is assumed to have detected all the master events present in the data, and is considered as the reference standard (zero missed events). Out of 897 events detected by the PSD method only 8 are false alarms and the rest are master events, of which 796 are identified as microseismic events and 93 as coherent signals mainly related to regional events (small earthquakes and their aftershocks) (Caffagni *et al.* 2015), as shown, for instance, in Fig. 5. The STA/LTA method, on the other hand, has detected 399 master events, consisting of 364 microseismic events and 35 coherent signals related to regional events, which

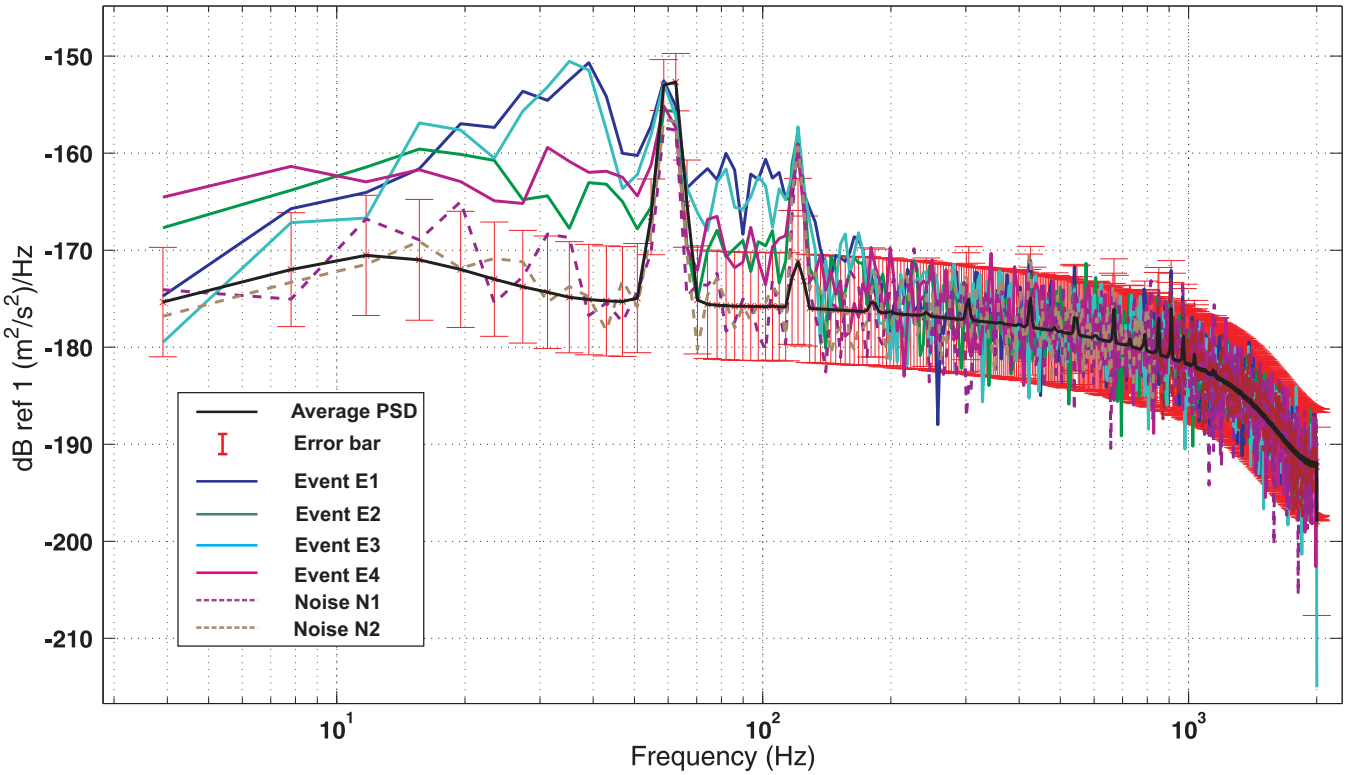

Figure 2. The average PSD curve (black) along with its standard deviations at each frequency (red bars), and the PSD estimates for four microseismic events E denoted by red boxes and two sample noise recordings N denoted by green boxes in the zoom-in view in Fig. 1.

only account for approximately 44.8 per cent of the total number of master events (that are assumed to have all been detected by the PSD method). There are a total number of 490 events that are missed by the STA/LTA method but detected by the PSD technique. Moreover, out of 412 events triggered by the STA/LTA algorithm 13 are false alarms, which are more than the number of false alarms in the PSD method. Therefore, the ratio of detected events over false triggers is improved significantly in the PSD method when compared to the STA/LTA technique.

Figs 6(b) and (e) show two raw segments of the vertical component data each including a potential weak microseismic event in the middle, which are obscured by the background noise. Therefore, they are not detectable by the STA/LTA technique even when applied to the data filtered with notch filters at the frequencies of 60 and 120 Hz. On the other hand, the modified PSD detection method has successfully detected these events due to their anomalous PSD estimate over some frequency band compared to the average noise PSD, as indicated by the time–frequency representations of the above-unity PSD misfit ratios (eq. 9) at the corresponding times shown in Figs 6(a) and (d), respectively. In order to ensure these are indeed microseismic events they are bandpassed over their dominant frequency band, [5 55] Hz, deduced from their time–frequency representations at the times of their existence. Figs 6(c) and (f) show the corresponding bandpassed *Z*-component time-series at all the geophone levels (RCV1 is the shallowest receiver and so on). The apparent velocities associated with these events are estimated to be around 3280 m s^{-1} and 3340 m s^{-1}, respectively, which are similar to the available average sonic *P*-wave velocity in the formations surrounding the monitoring well (Eaton *et al.* 2014). Therefore, their apparent velocities and their coherencies at all geophone levels confirm that they are microseismic events. The times at which these detections are made via the PSD method on the shallowest receiver are denoted by red arrows. Filtering the data over the frequency range of [5 55] Hz causes these events to stand out of the background noise. Therefore, when applied to the data filtered in this frequency range, the STA/LTA method succeeds in detecting these two events.

These two events have PSD criteria that are larger by 2 and 1.8 times the standard deviation of the noise model within this frequency range, respectively. Assuming a Gaussian probability distribution, this quantifies to probabilities only from 2.27 per cent to 3.6 per cent that these are due to random noise fluctuations (eq. 12).

The time–frequency representation of the measured PSD ratios for the whole 1-hr long segment (Figs 3a and b) shows that the frequency band over which the microseismic events are significantly dominant with respect to the noise is [5 55] Hz. The detected microseismic events have mostly PSD ratios between 2 and 8 in this frequency range that translate into 2.27 to 6.18E-14 per cent probability that they are due to noise (eq. 12). This can also help in designing suitable bandpass filters in order to better identify and analyse microseismic events.

The third row in Table 2 provides the number of master events, false alarms and missed events in the STA/LTA method when applied to the data filtered in the frequency range of [5 55] Hz deduced from the PSD technique. The performance of the STA/LTA method has been significantly improved when implemented to the data filtered over this frequency range. The number of detected master events has increased from 412 to 554, while the number of false alarms and missed events has reduced from 13 to 9 and from 490 to 335, respectively. The pronounced increase of number of detected coherent signals is mainly due to the fact that the dominant frequency band of the regional events that encompass most of these types of signals is [2 25] Hz. Therefore these events are enhanced significantly and stand out clearly after applying the optimal filter,

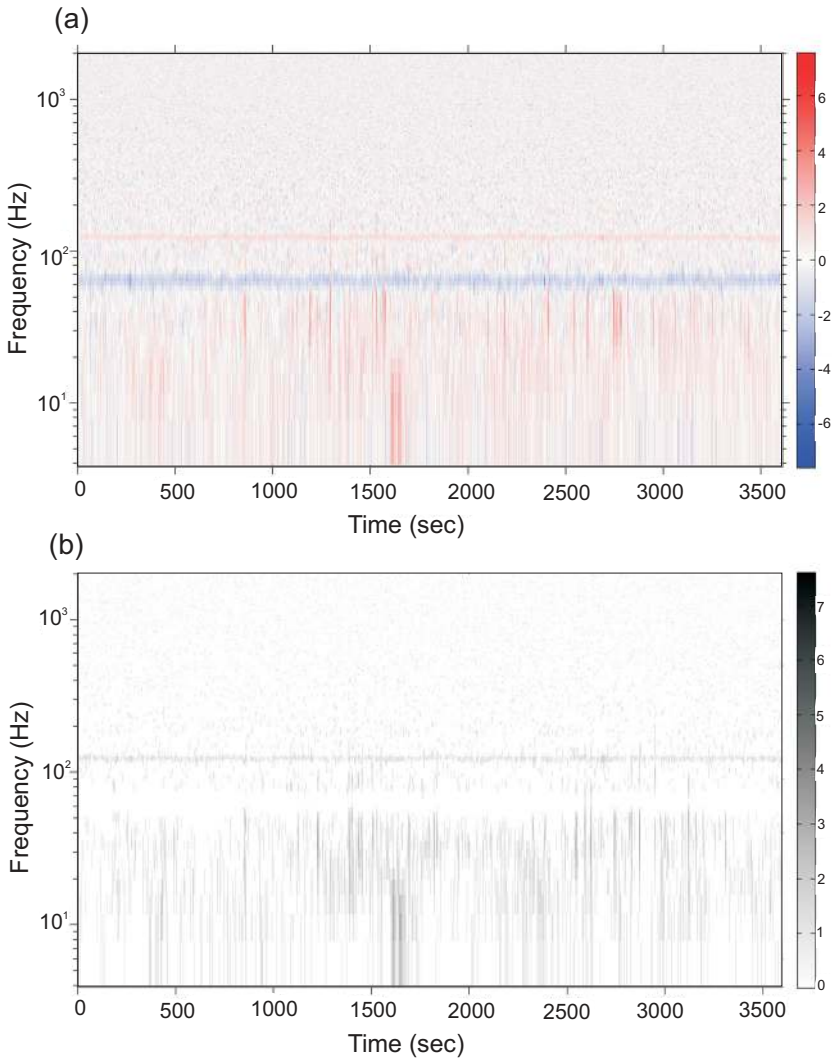

Figure 3. (a) The time–frequency representation of raw PSD ratios calculated using eq. (8). (b) The same as (a) for PSD ratios calculated using eq. (9). The microseismic events appear dominantly at the frequencies below 120 Hz. 120-Hz line is the first overtone of the removed 60-Hz electric noise.

resulting in a higher number of detected coherent signals. Despite improvements in the STA/LTA method after applying an optimal bandpass filter to the data, the number of detected master events only account for approximately 62.3 per cent of the total number of master events detected by the PSD technique when applied to the raw data. Also, the PSD technique still provides a marginally lower number of false alarms and a smaller number of missed events. Therefore, the PSD technique remains as the superior event detection algorithm although implemented on the unfiltered data.

Fig. 7 shows an example of a weak event that has been detected by the PSD method but is missed by the STA/LTA method applied to both the data filtered using notch filters at the frequencies of 60 and 120 Hz and the data bandpassed in the frequency range of [5 55] Hz. The comparable amplitude of the event with the background noise, even when the data are bandpassed between 5 and 55 Hz, causes the STA/LTA method to fail in detecting this event. However, the elevated spectral content of the event with respect to that of the background noise makes the PSD method succeed in detecting this weak event. An apparent velocity of 3450 m s^{-1} and coherency of the waveforms along the receiver array confirm that this is an event.

5 DISCUSSIONS

Our suggested event detection method uses a similar number of parameters as in the STA/LTA technique, namely a sliding window of pre-determined length and a detection threshold. As the PSD technique is based on the time–frequency representations, a trade-off between temporal and spectral resolutions should be considered when choosing the window length (Tary *et al.* 2015). The window length should be large enough to adequately account for long-period components of the signals and small enough to be able to make a distinction between closely-spaced events. In the PSD method, one could choose an absolute pre-set threshold for triggering (eq. 10 or 11) or a statistical one, in the sense that an event is triggered at any specific time once its likelihood to be due to noise only is less than a pre-selected value (eq. 12).

The PSD method can also be utilized for designing a more suitable bandpass filter for further microseismic data analyses whereas the STA/LTA method usually requires bandpassed data prior to event detection. The PSD algorithm is also insensitive to variations in the signal frequency content. However, it does assume stationary background noise conditions (Vaezi & van der Baan 2014).

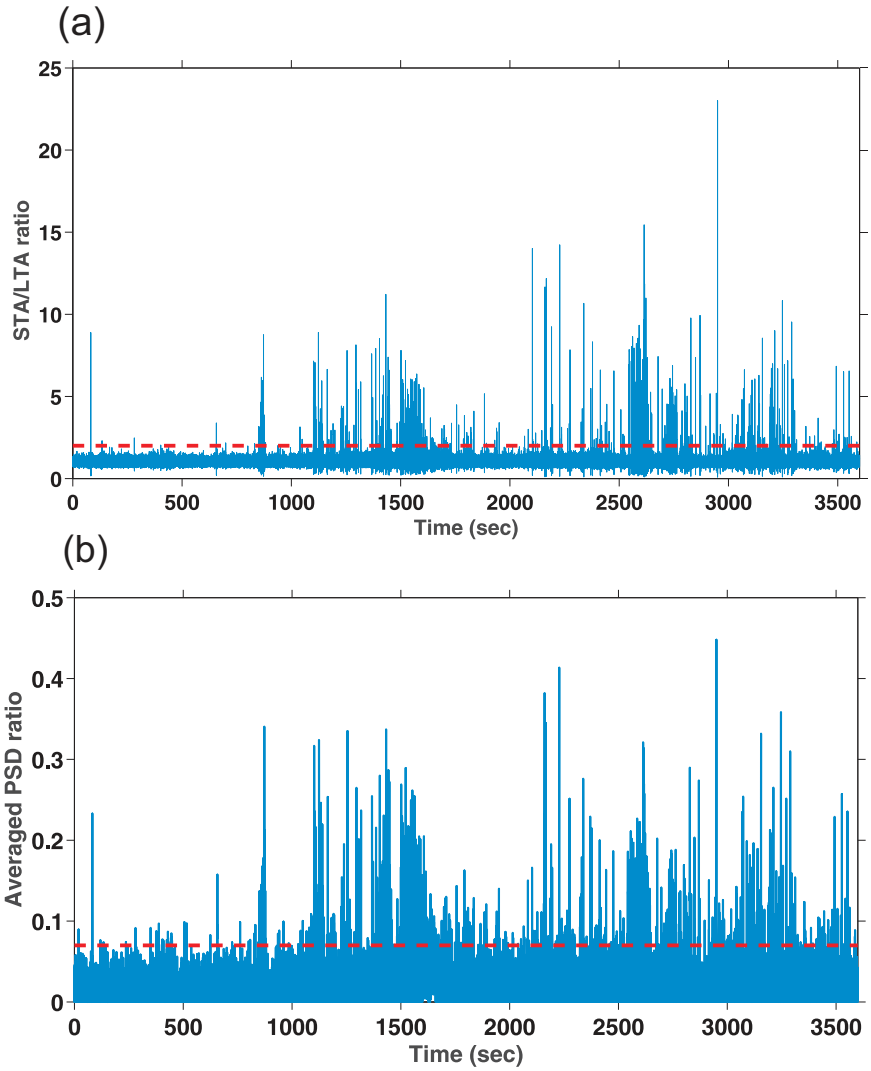

Figure 4. (a) The STA/LTA ratio calculated using the parameters listed in Table 1. (b) The PSD detection criterion calculated by eq. (10) using the parameters listed in Table 1. The red dashed lines represent the detection threshold for each method.

Table 2. The number of master events, false alarms and missed events in the PSD method when applied to the raw data shown in Fig. 1 (first row) and the STA/LTA method when applied to the same data filtered with two narrow notch filters at the frequencies of 60 and 120 Hz (second row). The third row presents similar variables for the STA/LTA method when applied to the same data filtered in the frequency band of [5 55] Hz. Compared to the STA/LTA method, the PSD method not only detects more events but also provides less false alarms and missed events. Bandpassing the data over the frequency band deduced from the PSD method improves the performance of STA/LTA method.

	Master events			
	Microseismic events	Other coherent signals	False alarms	Missed events
PSD method (raw data)	796	93	8	0
STA/LTA method (notch-filtered data)	364	35	13	490
STA/LTA method (filtered data)	475	79	9	335

Both the STA/LTA and PSD techniques can be applied in a multichannel strategy in which a voting scheme is used to trigger events (Trnkoczy 2002). This way an event is declared once the total number of votes (weights) exceeds a given pre-set value. The spectral characteristics of the two horizontal channels may be significantly different from that of the vertical channel. Therefore, it is suggested that the PSD method is first applied separately to different components before combining the votes from different channels.

Both methods are incoherent (with respect to the background noise) energy detectors, meaning that triggered events may not correspond to microseismic events but other incoherent signals or even incoherent noise (e.g., spikes, bursts) which represent locally incoherent amplitudes (or energy or envelope) in the STA/LTA method or display sufficiently elevated spectral content over a frequency range in the PSD method. Therefore, a manual quality control is required to ensure that the declared events are indeed microseismic events as well as discard the false triggers. The reduced number of

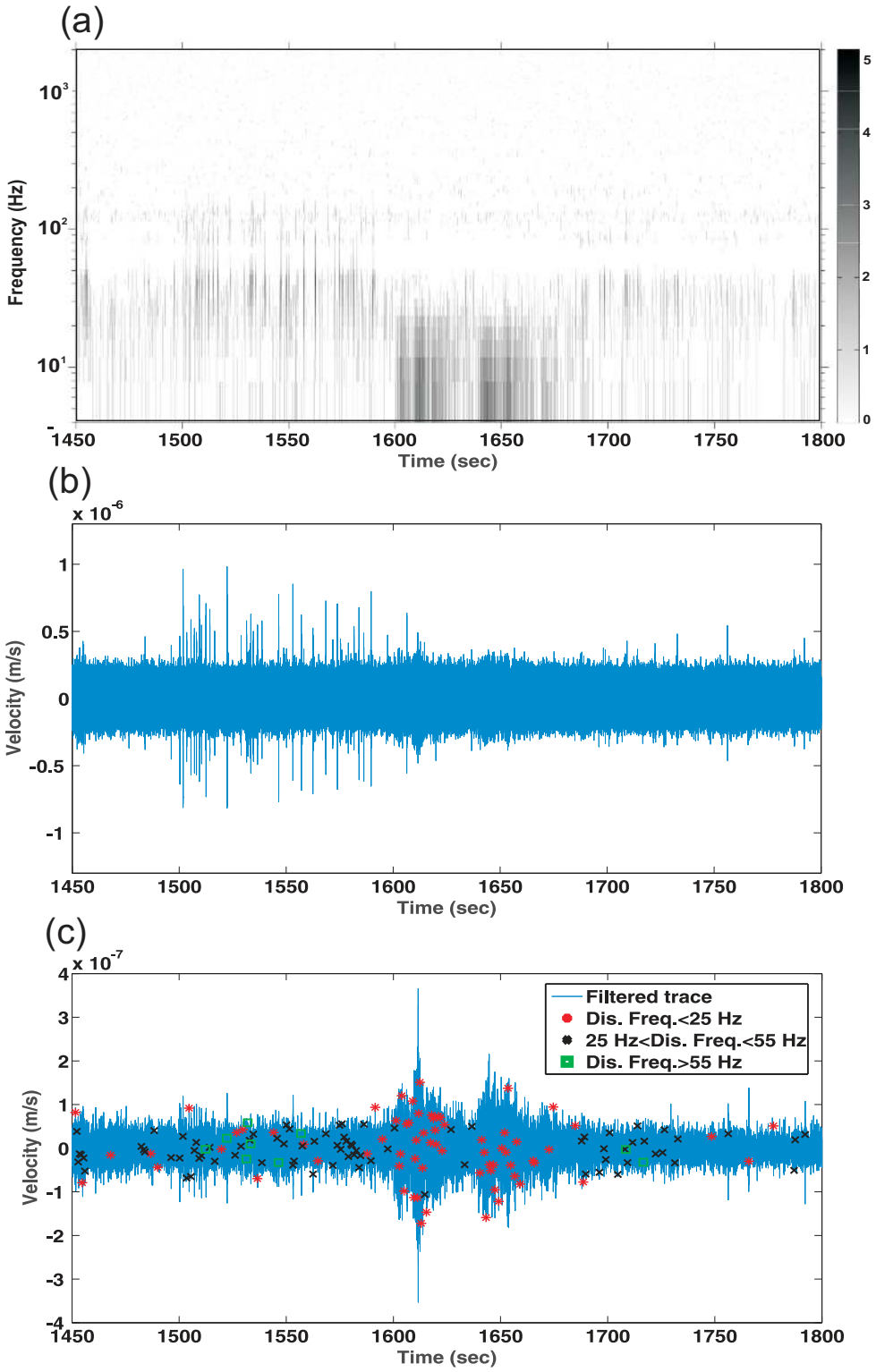

Figure 5. (a) The time–frequency representation of the above-unity PSD misfit ratios (eq. 9) around some low-frequency signals that are detected by the PSD method. These signals are interpreted to arise mostly from small regional earthquakes observed in the data. (b) The associated raw data. (c) The same data after applying a bandpass filter over the frequency range of [2 25] Hz. The master events detected by the PSD method at the time of appearance of these regional earthquakes are dominated by those of discriminating frequencies (Dis. Freq.) below 25 Hz (red stars). The detected events of discriminating frequencies in the range of [25 55] Hz and above 55 Hz are mostly observed before and after these earthquakes and are denoted by black crosses and green squares. Compared with the STA/LTA method, the PSD method is significantly more sensitive to the coherent signal portions of length 0.25 s within such events and detects a greater number of such signals (93 coherent events). This is because their PSDs are sufficiently stronger than the average PSD over their dominant frequency range. The STS/LTA, however, is only sensitive to abrupt amplitude changes and detects only 35 energetic signals within these events.

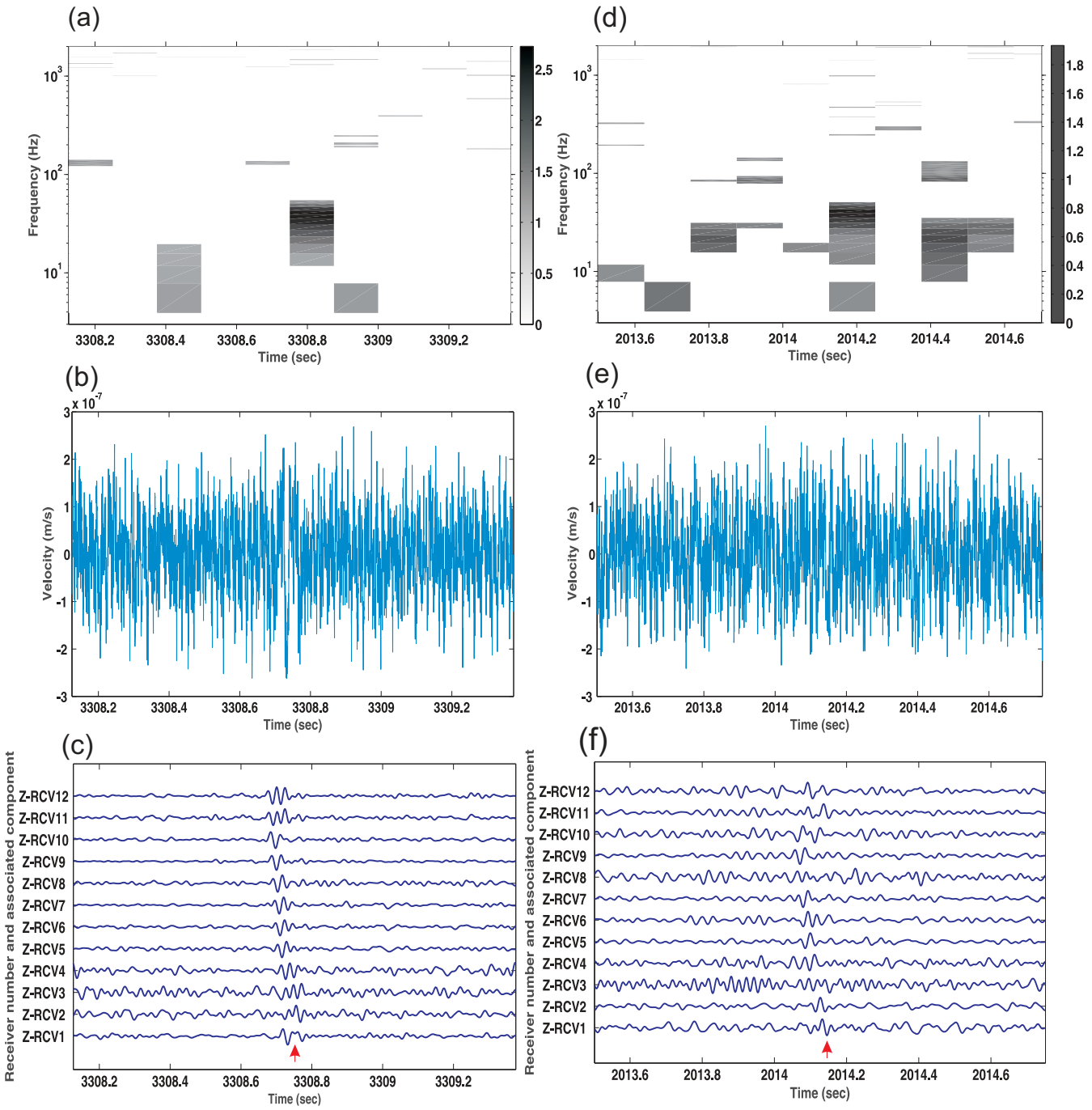

Figure 6. (a,d) The time–frequency representation of the above-unity PSD misfit ratios (eq. 9) in the proximity of two events detected by PSD method and missed by the STA/LTA method when the latter is applied to the data filtered with notch filters at the frequencies of 60 and 120 Hz. These events are also detected by the STA/LTA method applied to the data bandpassed between [5 55] Hz. The events are detected to be in the middle of these time windows. (b,e) The corresponding raw (unfiltered) waveforms of these two events on receiver 1. (c,f) The corresponding filtered time-series over the frequency range of [5 55] Hz at all geophone levels. The red arrows show the detection times obtained by the PSD technique.

false alarms for the PSD method is important since it reduces the time spent on manual quality control.

Although the PSD method outperforms the STA/LTA method in detecting a higher number of weaker events, there are situations in which the PSD method may lead to false positives. An example of such situations is the occurrence of transient or time-varying noise which cannot be captured by the stationary background noise assumption. These can be caused by diurnal variations in the energy levels or originate from ambient noise sources (e.g. traffic, etc.). Electric noise (spikes in the signal) also lies in this category (Figs 8a–c). A possible remedy for the case of diurnal variations is to analyse the daily and nightly data separately by calculating separate average PSDs for each case and, therefore, setting different PSD ratio thresholds, respectively. Another example where the PSD method may result in false event declarations is when a local energy increase either related or unrelated to microseismic activities is detected on one receiver which may not be consistent with the records on other receivers in the array, or it is observed on a single receiver

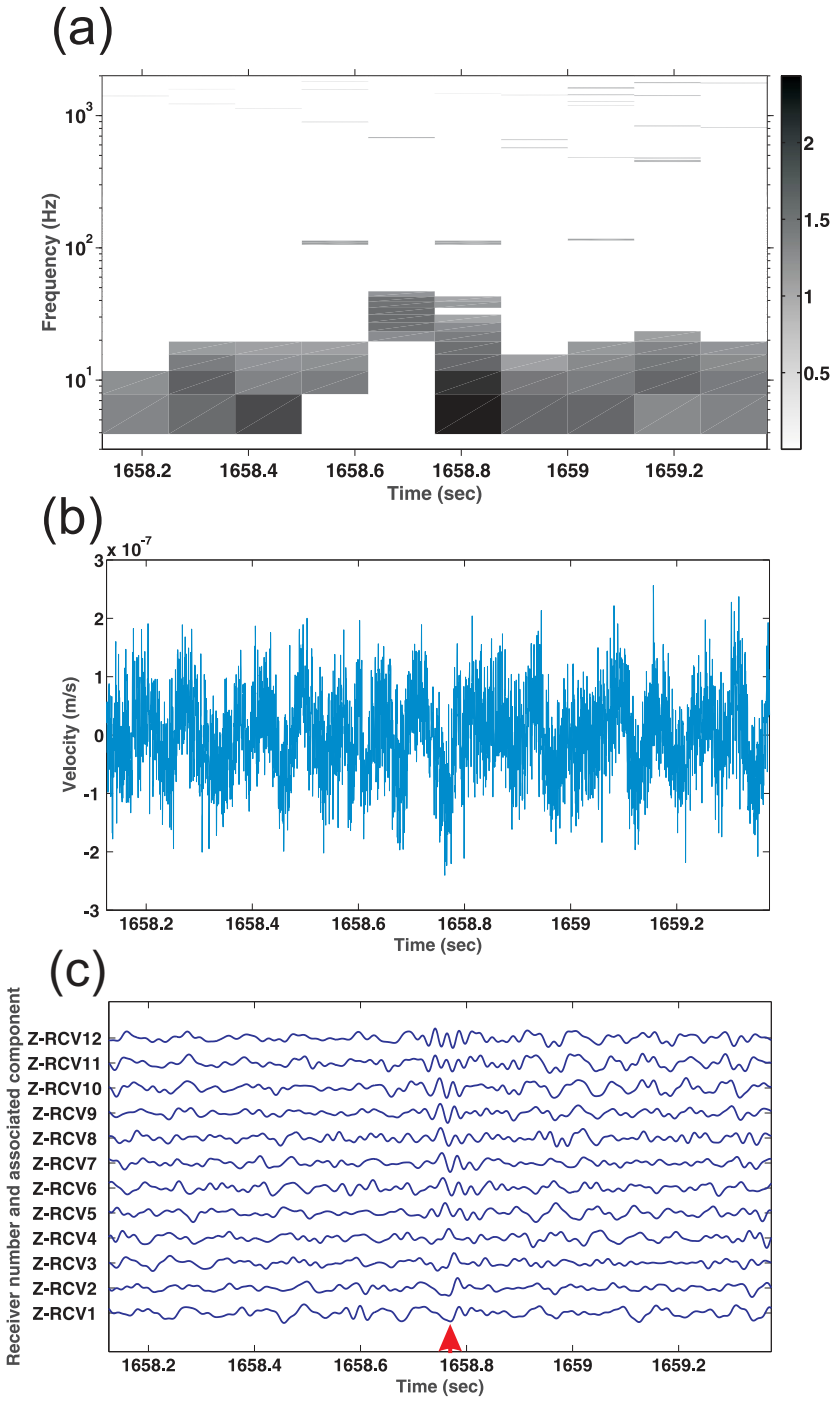

Figure 7. (a) The time–frequency representation of the above-unity PSD misfit ratios (eq. 9) in the proximity of an event detected by PSD method and missed by the STA/LTA method, no matter whether the latter is applied to the data filtered with notch filters at the frequencies of 60 Hz and 120 Hz or to the data filtered over the frequency range of [5 55] Hz. The event is detected to be in the middle of this time window. (b) The corresponding raw (unfiltered) waveform of this event on receiver 1. (c) The corresponding filtered time-series over the frequency range of [5 55] Hz at all geophone levels. The red arrow shows the event detection time obtained by the PSD technique.

only (Figs 8d–f). As the events are visually inspected using the array records, such detections due to locally elevated spectral energy levels only on an individual receiver are deemed false alarms as well. Furthermore, unusually large noise fluctuations are also undesired for the PSD method.

Among the 8 false alarms detected by the PSD method applied to our 1-hr long data set one is related to a transient (burst) noise and seven are related to features such as microseismic events or non-stationary noise which are detected on a single receiver only. Figs 8(a)–(c) show the burst, where its high amplitude and anomalously strong spectral content, especially over the frequency range of [7 200] Hz, causes it to be detected as an event via the PSD technique. However, the visual inspection using geophones at all levels (Fig. 8c) shows that this feature appears

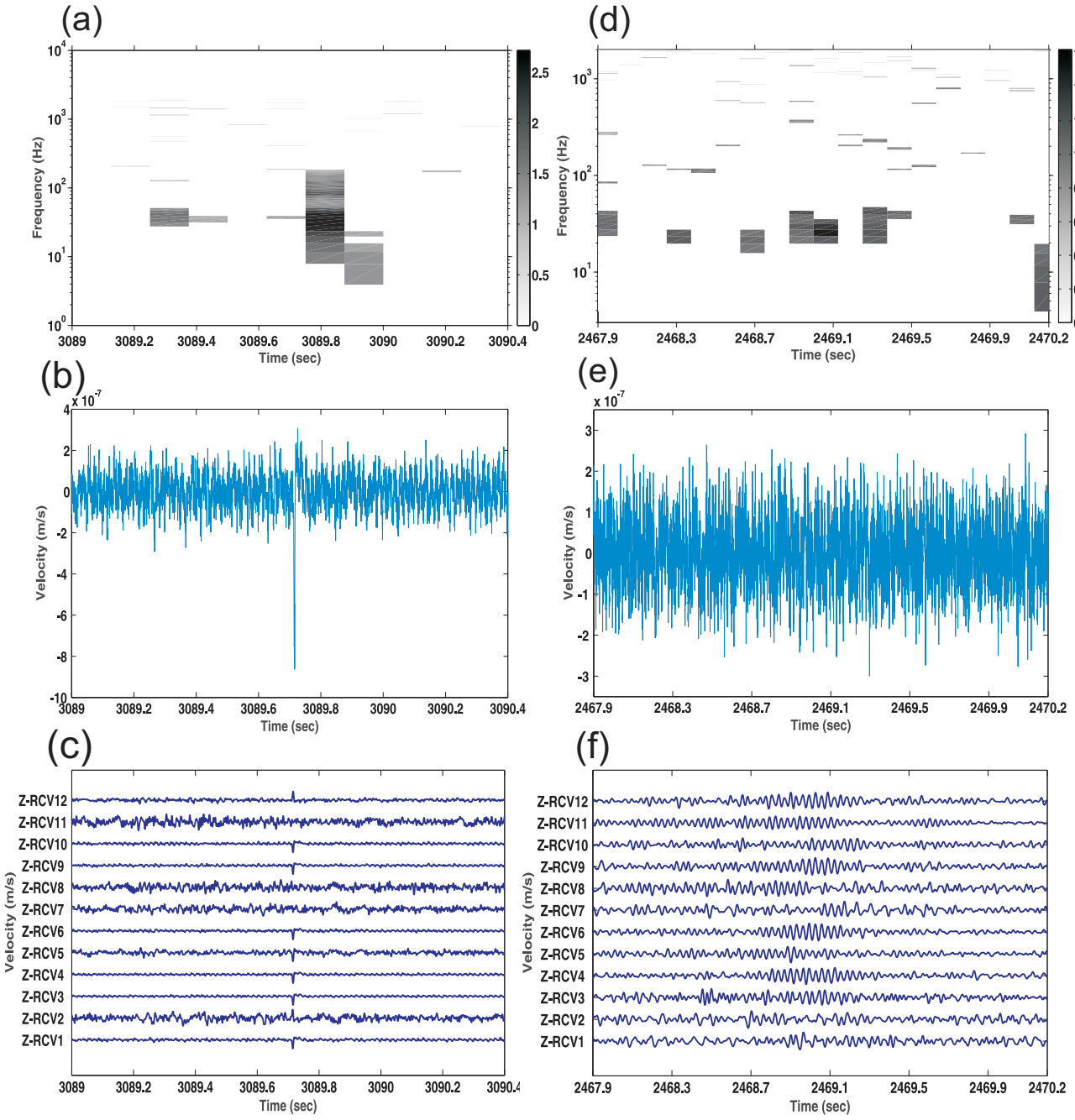

Figure 8. (a–c) Time–frequency representation of the PSD ratios, associated raw data on receiver 1 and the corresponding time-series filtered between 7 and 200 Hz on all geophones, respectively, for a spiky noise feature. The PSD technique picks up this false alarm due to this coherent nature. (d–f) Time–frequency representation of the PSD ratios, associated raw data on receiver 1 and the corresponding time-series filtered between 10 and 50 Hz on all geophones, respectively, for a second false alarm. Manual inspection on all geophone levels and lack of coherency along the array records suggests that this feature is most likely related to a local non-stationary energy variation as opposed to a microseismic event.

almost instantaneously on all geophones with differing polarities that can be due to instrument glitches or of other sources. Therefore, it is discarded as a false alarm during the manual quality control.

Figs 8(d)–(f) show an example where the PSD method detects an event when applied to the data on receiver 1. However, the manual quality control of this feature on geophone array shows no coherency along the array but only some local non-stationary increase in the energy level on other geophones. Therefore, this feature is also considered as a false alarm.

In this paper we focused on event detection. We did not investigate how suitable the PSD technique is for onset-time picking. Onset-time picking and event detection are two different concepts. The former includes specifying the exact arrival time of the events, whereas the latter only quantifies the likelihood of the presence of events. When its parameters are well set, the STA/LTA technique seems to better determine the onset times, while the PSD method works best in identifying the presence of an event. On the other hand, the PSD method is likely to perform better in detection of emerging events where the gradual amplitude increase often makes

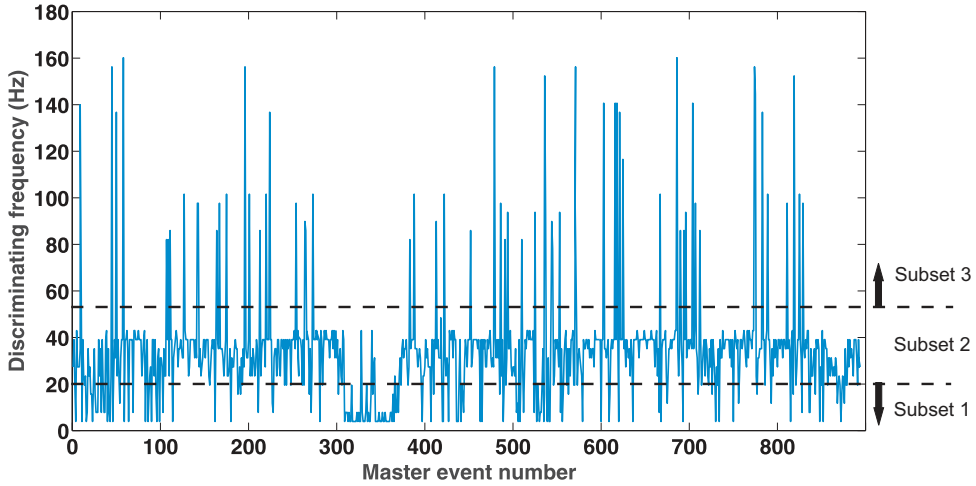

Figure 9. The discriminating frequencies corresponding to each master event detected by the PSD technique. The events can be categorized into three different event subsets based on the value of their discriminating frequencies, subsets 1 to 3, associated with events with discriminating frequency below 20 Hz, between 20 and 55 Hz and above 55 Hz, respectively.

the STA/LTA method fail. This can be explained by the fact that the PSD method is insensitive to the phase of the event, that is, an event can be detected as long as its spectral content is statistically large enough compared with the average PSD estimate, no matter whether the event is a minimum-, maximum- or a zero-phase event (that is, has a front-loaded, end-loaded or symmetric waveform). The STA/LTA method, on the other hand, is generally a minimum-phase event detector (that is, with most energy at the start of the arrival). One possible scheme to ensure superior performance is thus to start with the PSD technique for triggering, use the detected frequency range for bandpass filtering and then employ the STA/LTA or another picking method to detect the arrival onsets.

The PSD technique also provides useful information for event classification or identification since it explicitly reveals the signal frequency content. Fig. 9 shows the 'discriminating frequencies' for each of the 889 master events detected by the PSD method. The discriminating frequency of an event is here defined as the frequency at which the normalized PSD ($u_t(f)$ in eq. 8) has its maximum value at the corresponding time of the event. Three different event subsets associated with three distinct ranges of discriminating frequencies can roughly be identified: low-frequency events at the frequencies below 20 Hz which are mostly related to regional events (Fig. 5), intermediate-frequency microseismic events in the frequency range of [20 55] Hz which include the majority of detected master events and high-frequency microseismic events at the frequencies above 55 Hz. Therefore, we propose that the PSD method can further be used for event cluster analysis and phase identification (Shumway 2003; Fagan *et al.* 2013; Anderson *et al.* 2010; Langer *et al.* 2006; Scarpetta *et al.* 2005). Note that the short-wavelength step-wise fluctuations observed in the discriminating frequencies are approximately equal to 4 Hz, which is the frequency step in the PSD technique, as we have used 0.25 s long moving windows.

6 CONCLUSIONS

The PSD technique outperforms the STA/LTA method by detecting a higher number of weak microseismic events that are obscured by the background noise. When applied to the unfiltered data, the PSD method not only detects approximately 55.2 per cent more master events than the STA/LTA method applied to the data filtered by notch filters at the frequencies of 60 Hz and 120 Hz, but also reduces the number of false alarms and missed events. The PSD method has the advantage over the STA/LTA method that no prior bandpass filtering is required to enhance the S/N and also permits detection of signals with characteristically different frequency contents if the background noise spectrum is stationary. Even if the STA/LTA technique is applied to optimally filtered data, the PSD method still detects approximately 37.7 per cent more master events with a similar number of false alarms. Therefore, the PSD method remains as the superior event detection algorithm to the STA/LTA technique.

ACKNOWLEDGEMENTS

We thank the sponsors of the Microseismic Industry Consortium for financial support, and Neil Spriggs for discussions. We would also like to thank Honn Kao and another anonymous reviewer for their valuable comments and suggestions.

REFERENCES

Allen, R.V., 1978. Automatic earthquake recognition and timing from single traces, *Bull. seism. Soc. Am.,* **68,** 1521–1532.

Anderson, D.N. *et al.*, 2010. Seismic event identification, *WIREs Comp. Stat.,* **2,** 414–432.

Andrews, L.C., 1997. Special Functions of Mathematics for Engineers, SPIE Press, doi:10.1117/3.270709, eISBN: 9780819478467, pp. 109–110.

Caffagni, E., Eaton, D., van der Baan, M. & Jones, J.P., 2015. Regional seismicity: A potential pitfall for identification of long-period long-duration events, *Geophysics,* **80**(1), A1–A5.

Das, I. & Zoback, M.D., 2013. Long-period, long-duration seismic events during hydraulic stimulation of shale and tight-gas reservoirs—Part 1. Waveform characteristics, *Geophysics,* **78**(6), KS97–KS108.

Earle, P. & Shearer, P., 1994. Characterization of global seismograms using an automatic picking algorithm, *Bull. seism. Soc. Am.,* **84**(2), 366–376.

Eaton, D., Caffagni, E., Rafiq, A., Van der Baan, M., Roche, V. & Matthews, L., 2014. Passive seismic monitoring and integrated geomechanical analysis of a tight-sand reservoir during hydraulic-fracture treatment, flowback and production, in *Unconventional Resources Technology Conference,* Society of Petroleum Engineers, Denver, CO, doi:10.15530/utrec-2014-1929223.

Ewing, W.M., Jardetzky, W.S. & Press, F., 1957. *Elastic waves in layered media,* McGraw-Hill Book Company Inc., New York.

Fagan, D., Van wijk, K. & Rutledge, J., 2013. Clustering revisited: A spectral analysis of microseismic events, *Geophysics,* **78**(2), 568–571.

Harris, F., 1978. On the use of windows for harmonic analysis with the discrete Fourier transform, *Proc. IEEE,* **66,** 51–83.

Langer, H., Falsaperla, S., Powell, T. & Thompson, G., 2006. Automatic classification and a-posteriori analysis of seismic event identification at Soufrière Hills volcano, Montserrat, *J. Volc. Geotherm. Res.,* **153,** 1–10.

Lee, A.W., 1935. On the direction and approach of microseismic waves, *Phil. Trans. R. Soc. Lond., A.,* **149,** 183–199.

Maxwell, S.C., White, D.J. & Fabriol, H., 2004. Passive seismic imaging of CO_2 sequestration at Weyburn, in *74th Annual International Meeting, SEG, Expanded Abstracts,* **23,** 568–571, doi:10.1190/1.1842409.

Maxwell, S.C., Rutledge, J., Jones, R. & Fehler, M., 2010. Petroleum reservoir characterization using downhole microseismic monitoring, *Geophysics,* **75,** 75A129–75A137.

McEvilly, T.V. & Majer, E.L., 1982. ASP: An automated seismic processor for micro-earthquake networks, *Bull. seism. Soc. Am.,* **72,** 303–325.

McNamara, D.E. & Buland, R.P., 2004. Ambient noise levels in the continental United States, *Bull. seism. Soc. Am.,* **94,** 1517–1527.

Park, J., Lindberg, C.R. & Vernon III, F.L., 1987. Multitaper spectral analysis of high-frequency seismograms, *J. Geophys. Res.,* **92,** 12 675–12 684.

Peterson, J., 1993. Observations and modeling of seismic background noise, USGS Open-File Report, pp. 093–322.

Phillips, W.S., Rutledge, J.T. & House, L., 2002. Induced microearthquake patterns in hydrocarbon and geothermal reservoirs: six case studies, *Pure appl. Geophys.,* **159,** 345–369.

Scarpetta, S., Giudicepietro, F., Ezin, E.C., Petrosino, S., Del Pezzo, E., Martini, M. & Marinaro, M., 2005. Automatic classification of seismic signals at Mt. Vesuvius volcano, Italy, using neural networks, *Bull. seism. Soc. Am.,* **95**(1), 185–196.

Shumway, R.H., 2003. Time-frequency clustering and discriminant analysis, *Stat. Probab. Lett.,* **63,** 307–314.

Swindell, S.W. & Snell, N.S., 1977. Station processor automatic signal detection system, phase I: final report, station processor software development: Texas Instruments final report No. ALEX (01)–FR–77–01, AFrAC contract number F08606–76–C–0025, Texas Instruments Inc., Dallas, TX.

Tary, J-B., Herrara, R.H., Han, J. & Van der Baan, M., 2015. Spectral estimation - What is new? What is next?, *Rev. Geophys.,* **52,** 723–749.

Thomson, D.J., Spectrum estimation and harmonic analysis, *Proc. IEEE,* **70,** 1055–1096.

Trnkoczy, A., 2002. Understanding and parameter setting of STA/LTA trigger algorithm, in *IASPEI New Manual of Seismological Observatory Practice,* **2**, pp. 01–20, ed. Bormann, P., doi:10.2312/GFZ.NMSOP-2_IS_8.1.

Vaezi, Y. & van der Baan, M., 2014. Analysis of instrument self-noise and microseismic event detection using power spectral density estimates, *Geophys. J. Int.,* **197**(2), 1076–1089.

van der Baan, M., Eaton, D.W. & Dusseault, M., 2013. Microseismic monitoring developments in hydraulic fracture stimulation, in *Effective and sustainable hydraulic fracturing: InTech,* pp. 439–466, eds Bunger, A.P., McLennan, J. & Jeffrey, R., doi:10.5772/56444.

Warpinski, N.R., 2009. Microseismic monitoring: inside and out, *J. Pet. Technol.,* **61,** 80–85, doi:10.2118/118537-MS.

Welch, P.D., 1967. The use of fast Fourier transform for the estimation of power spectra: a method based on time averaging over short, modified periodograms, *IEEE Trans. Audio Electroacoust.,* **15,** 70–73, doi:10.1109/TAU.1967.1161901.

Withers, M., Aster, R., Young, C., Beiriger, J., Harris, M., Moore, S. & Trujillo, J., 1998. A comparison of select trigger algorithms for automated global seismic phase and event detection, *Bull. seism. Soc. Am.,* **88,** 095–106.